UNITED STATES
DEPARTMENT OF COMMERCE
NATIONAL INSTITUTE OF STANDARDS
AND TECHNOLOGY



*NIST Technical Note 1335*

# Generating Standard Reference Electromagnetic Fields in the NIST Anechoic Chamber, 0.2 to 40 GHz

D.A. Hill
M. Kanda
E.B. Larsen
G.H. Koepke
R.D. Orr

# Generating Standard Reference Electromagnetic Fields in the NIST Anechoic Chamber, 0.2 to 40 GHz

D.A. Hill
M. Kanda
E.B. Larsen
G.H. Koepke
R.D. Orr

Electromagnetic Fields Division
Center for Electronics and Electrical Engineering
National Engineering Laboratory
National Institute of Standards and Technology
Boulder, Colorado 80303-3328

U.S. DEPARTMENT OF COMMERCE, Robert A. Mosbacher, Secretary
NATIONAL INSTITUTE OF STANDARDS AND TECHNOLOGY, John W. Lyons, Director
Issued March 1990

National Institute of Standards and Technology Technical Note 1335
Natl. Inst. Stand. Technol., Tech. Note 1335, 48 pages (Mar. 1990)
CODEN;NTNOEF

U.S. GOVERNMENT PRINTING OFFICE
WASHINGTON: 1990

For sale by the Superintendent of Documents, U.S. Government Printing Office, Washington, DC 20402-9325

CONTENTS

Page

Abstract....1

1. INTRODUCTION....1

2. DESCRIPTION AND EVALUATION OF THE NIST RF ANECHOIC CHAMBER....2

3. DESCRIPTION AND GAIN OF THE STANDARD TRANSMITTING ANTENNAS....5
   3.1 Open-Ended Waveguides....5
   3.2 Pyramidal Horns....6

4. MEASUREMENT OF THE RF POWER DELIVERED TO THE TRANSMITTING ANTENNA....9
   4.1 Present Method....9
   4.2 Calibration of the Present RF Power Delivery System....11

5. COMPUTATION AND UNCERTAINTY OF THE CHAMBER FIELD MAGNITUDE....12

6. PROCEDURE FOR GENERATING A STANDARD FIELD....14

7. PLANNED IMPROVEMENTS IN THE ANECHOIC CHAMBER SYSTEM....15
   7.1 Transmitting Antenna Positioner....15
   7.2 Advanced Measurement Software....16
   7.3 Control Charts and Support Software....16
   7.4 Control Standards....16
   7.5 Detailed Uncertainty Analysis....16

8. CONCLUSIONS....17

9. REFERENCES....17

GENERATING STANDARD REFERENCE ELECTROMAGNETIC FIELDS IN THE NIST ANECHOIC CHAMBER, 0.2 TO 40 GHZ

D.A. Hill, M. Kanda, E.B. Larsen, G.H. Koepke, and R.D. Orr

Electromagnetic Fields Division
National Institute of Standards and Technology
Boulder, CO 80303

The NIST anechoic chamber is used to generate standard (known) EM fields for frequencies from 200 MHz to 40 GHz. The transmitting antennas used are open-ended rectangular waveguides from 200 to 500 MHz and pyramidal horns from 450 MHz to 40 GHz. The uncertainty in the electric field is currently estimated to be ± 1.0 dB. A number of changes and additions are planned to improve the accuracy, repeatability, and efficiency of the system.

Key words: anechoic chamber; delivered power; near-field gain; open-ended waveguide; pyramidal horn; standard field.

## 1. INTRODUCTION

The National Institute of Standards and Technology (NIST) radio frequency (rf) anechoic chamber is one of several facilities maintained by NIST for the purpose of generating a standard (known) electromagnetic (EM) field. This chamber can be used for calibrating antennas, EM probes, and rf radiation hazard monitors and for research purposes. The anechoic chamber provides calculable EM fields over the frequency range of 200 MHz to 40 GHz. The uncertainty of the standard field is now ± 1 dB. A side-view sketch of the NIST anechoic chamber is given in figure 1.

There are three main parts to the NIST standard-field system: (1) an anechoic chamber, which is described in Section 2 of this report; (2) several standard-gain transmitting antennas, described in Section 3; and (3) an rf power delivery system which is discussed in Section 4. The antennas are used to radiate a beam of EM energy into the anechoic chamber, which is a shielded metal-clad room covered internally with rf absorbers. Thus, outside ambient EM energy is greatly attenuated, and energy beamed into the chamber will be absorbed rather than reflected and scattered from the walls.

The electric field strength at a specific distance from the radiating antenna is calculated from measurements of the power delivered to the transmitting antenna and a knowledge of the gain of the antenna as a function of frequency and distance to the field point. The equation used to calculate the electric field E on the boresight axis of the transmitting antenna is

$$E = [\eta_0 P_{del} G/(4\pi)]^{1/2}/d = (30\ PG)^{1/2}/d, \tag{1}$$

where E = electric field strength, V/m,

$P_{del}$ = P = net power delivered to the transmitting antenna, W,

$\eta_0$ = free-space impedance ≈ 120 $\pi$, Ω,

G = gain of the transmitting antenna at the given frequency and distance, and

d = distance from the center of the aperture of the transmitting antenna (horn or OEG) to the on-axis field point, m.

Control charts are being implemented to monitor and evaluate the overall performance of the field generating system used in the anechoic chamber, so that quality checks which are made each time the facility is used will reveal whether the system is functioning properly . Separate control charts will also be maintained for the rf power delivery system. These serve two purposes: (1) to check on the proper functioning of the transmitting system and (2) to develop more accurate values of forward and reverse coupling ratios for the directional coupler used in measuring the net power delivered to the transmitting antenna.

## 2. DESCRIPTION AND EVALUATION OF THE NIST RF ANECHOIC CHAMBER

The anechoic chamber shown in figure 1 is constructed within a metal-shielded room approximately 4.9 m (16 ft) high by 6.7 m (22 ft) wide by 8.53 m (28 ft) long. It is lined with rf absorbing material on the interior walls, ceiling, and floor to reduce electromagnetic reflections. The absorber covers all chamber surfaces except for exhaust fans in two side walls, an opening in the front wall where the transmitting antenna is placed, and metal rails on the floor. These precision rails support a rolling equipment cart on which the receiving antenna under test (AUT) is mounted, together with auxiliary equipment such as an antenna rotator/positioner, driver motors for moving the cart, and rf absorbers on the front wall of the cart. There is a gap 0.2 m wide in the absorbers on the floor to accomodate each of the two rails. The AUT is mounted inside the chamber on this equipment cart, which permits movement of the AUT parallel to the boresight axis of the standard transmitting antenna. The transmitting antenna is either a pyramidal horn or a rectangular open-ended waveguide (OEG) and is mounted on a carriage outside the anechoic chamber, with its radiating aperture located approximately 0.6 m inside the plane of the absorber tips on the front wall of the chamber.

The equipment cart can be moved manually or positioned with computer-controlled stepping motors to within ± 2 mm along the 6 m length of the rails. The receiving antenna is installed in a specially fabricated dielectric fixture placed on or affixed to the cart. The antenna rotator can be used to make receiving antenna pattern measurements, but pattern measurements will not be covered in this report.

The response of the AUT to an established standard field is monitored by voltage or power readouts from instruments placed on the chamber equipment cart. The response can be read by computer-controlled acquisition through an IEEE 488 bus. The data are conveyed through fiber optic lines which extend from the cart to a computer located in an adjacent room. Fiber optic lines are used because they are essentially transparent to rf energy and immune to interference or other pickup from fields within the chamber.

The absorber used is a commercially available carbon-impregnated urethane foam with pyramidal points, as shown in figure 2. This material has reasonably good absorption at frequencies down to 200 MHz, especially for normal incidence, but is much better at higher frequencies. Two independent evaluations were made of the NIST anechoic chamber [1,2] by measuring the distortion of an electromagnetic field caused by reflections within the chamber.

In [1], the relative insertion loss between a standard-gain antenna and a probe antenna was measured along the boresight axis of the standard-gain antenna. The measurements were made at 20 frequencies from 175 MHz to 18 GHz and compared with theoretical, inverse-square curves. The theoretical, inverse-square curves were fitted to the measured curves at a distance of 1 m. The difference between the measured and theoretical insertion loss was assumed to be caused by chamber reflection error, and the ranges of differences are shown in table 1. A maximum difference range of - 0.6 to 0.5 dB occurred at 229 MHz, but at 18 GHz the variation was only ± 0.04 dB. Insertion loss curves as a function of antenna separation are shown in figures 3-7. Standing waves due to chamber reflections are most evident at the lower frequencies.

Measurements were made of electric field components in the anechoic chamber [2] using a calibrated isotropic NIST probe having three dipoles mutually orthogonal (designated EFM-3). These data were taken along the boresight axis of the transmitting antenna and also along other parallel axes. The off boresight data give an indication of error in standard values as a function of displacement from the boresight axis and the deviation from boresight field value that would occur at off-axis points on a large receiving antenna or device under test. The off-axis field reduction is primarily a function of the pattern of the transmitting antenna, while standing-wave patterns in field strength are due to multi-path interference caused by chamber reflections.

In the experiments described in [2], a 2 m × 2 m wooden frame was mounted vertically on the chamber receiving cart in a plane perpendicular to the beam from the transmitting antenna. Locations of the receiving probe on the frame are shown in figure 8. Typical data of measured field strength, labeled according to probe position, are given in figure 9, and standard deviations of the electric field are shown in figure 10. The measured off-boresight errors are summarized in table 2 for frequencies from 250 to 1000 MHz. The data indicate that for frequencies below 1000 MHz, a 25 cm displacement from the boresight axis could cause a field strength error as great as ± 0.5 dB. However, the laser alignment system in the anechoic chamber makes it a simple matter to align a receiving probe within ± 1 cm of the boresight axis, over a range in antenna separation distance of 1 to 6 m.

Experimental results in [2] indicate that during a 5 m traverse in distance an unwanted lateral displacement of ± 1 cm at the receiving probe would cause a field strength deviation from the boresight value by much less than 0.1 dB.

The experiments described in [1] and [2] were performed to evaluate the uncertainty in computed values of electric field in the anechoic chamber caused by chamber reflections and uncertainty in probe position. The data in [1] show that a typical boresight position uncertainty of ± 1 cm makes a negligible contribution to the field strength uncertainties reported in table 1. The boresight scans of electric field versus distance given in [2] are consistent with those reported in [1], both in shape and amount of standing-wave distortion.

## 3. DESCRIPTION AND GAIN OF THE STANDARD TRANSMITTING ANTENNAS

Two types of antennas are used in the NIST anechoic chamber as standard transmitting antennas in the 0.2-40 GHz frequency range: (1) open-ended rectangular waveguides (OEGs) at frequencies from 200 to 500 MHz and (2) pyramidal standard-gain horns from 450 MHz to 40 GHz. Both antenna types radiate a calculable, linearly polarized electric field on boresight.

### 3.1 Open-Ended Waveguides

An OEG of width w and height h is shown in figure 11. The approximate far-field gain, G, of an OEG having a two-to-one aspect ratio (w = 2h) is calculated at NIST from the equation [3]

$$G = 21.6\ Fw, \qquad (2)$$

where F is the frequency in GHz and w is the waveguide width (longer side) in meters. A list of the physical dimensions of the OEGs used at NIST is given in table 3. Two different OEGs are used to cover the frequency range 200 to 500 MHz.

The approximate gain expression in (2) was obtained by fitting an empirical equation [3] to data determined experimentally using a small indoor antenna range at NIST [4]. The gain of a WR-430 OEG was measured in the frequency range of 1.7 to 2.6 GHz using two identical OEGs as a transmitter and receiver pair. A graph of the gain calculated from (2), for a transmitting WR-2100 OEG at 500 MHz, versus the gain obtained from field strength measurements using a calibrated short-dipole probe is shown in figure 12. The experimentally determined gain relationship of (2) is accurate at all distances greater than 1 m, except for cyclical variations caused by multi-path interference in the anechoic chamber. In general, (2) is accurate within ± 0.5 dB if the distance d from the OEG aperture to the field point is greater than 2w [3]. The frequency range where (2) is valid is the range for which the waveguide size is appropriate and only the $TE_{10}$ mode is propagating. We also assumed that corrections have been made for the small insertion loss of the waveguide between the power measurement point and the radiating aperture.

Possible near-zone corrections for the gain of OEGs have been discussed in [4] and [5]. However, the near-zone corrections for OEGs are much less than those of pyramidal horns because the electrical size of the aperture is smaller. Thus the far-field gain as given by (2) can be used without near-field correction for $d > 2w$.

New replacement OEGs at NIST are longer than those previously used. The extra length stabilizes the OEGs mechanically as they extend over the end of the transmitting antenna positioner table and gives the $TE_{10}$ mode a greater distance to form before reaching the radiating aperture.

### 3.2 Pyramidal Horns

The geometry of a pyramidal horn is shown in figure 13. The width and height of the rectangular aperture are a and b, and the slant lengths are $\ell_E$ and $\ell_H$. Jull's expression for the near-field gain G is [6,7]

$$G = \frac{32ab}{\pi\lambda^2} R_E R_H, \tag{3}$$

where $\lambda$ is the free-space wavelength, and $R_E$ and $R_H$ include the gain reduction due to the E and H plane flare of the horn as well as the effect of finite range. The gain reduction factors are

$$R_E = \frac{C^2(w) + S^2(w)}{w^2},$$

$$R_H = \frac{\pi^2\{[C(u) - C(v)]^2 + [S(u) - S(v)]^2\}}{4(u - v)^2}, \tag{4}$$

where $w = b/(2\lambda \ell'_E)^{1/2}$,

$$\left.\begin{matrix} u \\ v \end{matrix}\right\} = \frac{1}{a}(\lambda \ell'_H/2)^{1/2} \pm a/(2\lambda \ell'_H)^{1/2},$$

$$\ell'_E = \frac{d\ell_E}{d + \ell_E}, \quad \ell'_H = \frac{d\ell_H}{d + \ell_H},$$

and d is the on-axis distance from the aperture plane. The Fresnel integrals C and S are defined as

$$C(w) - jS(w) = \int_0^w \exp(-j\pi t^2/2)\, dt. \tag{5}$$

In our computer program for (3)-(5), we use the approximations of Boersma [8] to compute the Fresnel integrals, and we have checked our results with Jull's curves and tables for $R_E$ and $R_H$ [6,7]. Larsen and Ries [3] have derived polynomial fits for $R_E$ and $R_H$ that are easy to compute, and they are accurate for most cases of practical interest.

A comparison of the theoretical gain and the gain values determined experimentally in the anechoic chamber, as a function of distance, are shown in figure 14 for a frequency of 500 MHz and in figure 15 at 1000 MHz [3]. These figures show that there is less than 0.8 dB difference between the theoretical and measured gains for the separation distances used in calibrations at NIST, which range from 1 to 4 m from the horn aperture. The greatest difference encountered (0.8 dB) was for distances between 1 and 2 m from the large horn at 500 MHz. At other distances and frequencies the differences were generally less than 0.5 dB. Some of this difference is due to an estimated ± 0.5 dB uncertainty in measurement of the E-field with a $\lambda/2$ standard dipole. The uncertainty due to calculating G from (3) is approximately ± 0.4 dB for the distances and frequencies used in the NIST chamber. An additional uncertainty of ± 0.4 dB is caused by in-phase and out-of-phase reflections from the imperfect absorber and other objects.

More recently, near-field gain measurements from 18 to 40 GHz have been made in the NIST anechoic chamber using pairs of pyramidal horn antennas [9]. The gain as determined by the two-antenna method is [10]

$$G = \frac{4\pi d}{\lambda} (P_r/P_t)^{1/2}, \tag{6}$$

where d is the distance between the horn apertures, $P_t$ is the net power delivered to the transmitting horn, and $P_r$ is the received power. Normally (6) is used for the far-field gain, but here we also use (6) for the near-field gain. In figures 16-18, we show the theoretical and measured near-field gains as a function of distance d for frequencies of 18, 26.5, and 40 GHz [9]. The agreement between theory and measurements is better than in figures 14 and 15 for two reasons: (1) the two-antenna method eliminates the uncertainty caused by the $\lambda/2$ receiving dipole, and (2) the chamber reflections are very small at frequencies above 18 GHz [1]. The disadvantage of the two-antenna method is that the near-field gain is not quite the same as Jull's near-field gain [6,7] which is defined in terms of the on-axis electric field. However, the two quantities have been shown to agree quite well for separation distances of interest in generating standard fields [9].

## 4. MEASUREMENT OF THE RF POWER DELIVERED TO THE TRANSMITTING ANTENNA

In this section we describe the method currently used to determine the net power delivered to a transmitting antenna in the NIST anechoic chamber. A somewhat different method [10] has been proposed for possible future use, but this proposed method will not be covered here.

### 4.1 Present Method

The net power delivered to the transmitting antenna is now determined using a dual-directional coupler attached directly to the transmitting antenna, as shown in figure 19. The net power is calculated from power meter readings made at the two side arms of the directional coupler and from coupling ratios determined by previous calibrations using the equation

$$P_{del} = P_{inc} - P_{rfl}, \tag{7}$$

where $P_{del}$ = net power delivered to the transmitting antenna,

$P_{inc}$ = incident power at the antenna input terminal, and

$P_{rfl}$ = reflected power at the antenna input terminal.

In (7), the two quantities, $P_{inc}$ and $P_{rfl}$, are determined from measurements with 50-Ω power meters, using the two equations

$$P_{inc} = P_{fwd}\ 10^{(C_{fwd}/10\ +\ A/10)}, \tag{8}$$

$$P_{rfl} = P_{rev}\ 10^{(C_{rev}/10)}, \tag{9}$$

where $P_{fwd}$ = power meter reading of forward power at side arm 1 of the directional coupler, port 1 in figure 19,

$P_{rev}$ = power meter reading of reverse power at side arm 2 of the directional coupler, port 2 in figure 19,

$C_{fwd}$ = forward coupling ratio (in dB) of the directional coupler with respect to the output port of the coupler in figure 19,

A = insertion loss (in dB) of the calibrated forward attenuator pad, if used, and

$C_{rev}$ = reverse coupling ratio (in dB) of the directional coupler with respect to the output port of the coupler.

The 50-Ω power meters are calibrated by the NIST power calibration services.

$C_{fwd}$ in (8) must be measured in terms of the ratio of the power reading at side arm 1 (port 1) to the power accepted by a 50-Ω power meter connected at the output (port 4) of the directional coupler. Accurate measurements of power when using the NIST-calibrated power meters require that correction factors be applied to the power meter by means of a dial setting on the front panel of the power meter. This correction factor makes allowance for: (1) the measured efficiency of the bolometer mount of the power sensor, (2) any mismatch error in the power meter sensor caused by its impedance deviating from 50 Ω, and 3) errors associated with the dc portion of the power meter. The NIST calibration of this overall correction factor, in the frequency range of 0.2 to 2 GHz, has a total uncertainty of ± 0.5 %. The value of the total correction factor varies from about 90 to 100 %, depending on the signal frequency (and power to a minor degree). After the appropriate correction factor has been set on the power meter panel, the indicated power is correct to ± 0.5 %. When using the NIST standard gain transmitting antennas, which have a maximum standing wave ratio of 1.5, it is possible to measure $P_{del}$ with an uncertainty of ± 0.6 %. The additional 0.1 % in uncertainty is caused by taking the difference between the larger value of $P_{inc}$ and the relatively small value of $P_{rfl}$.

The NIST measurements of the two coupling ratios, $C_{fwd}$ and $C_{rev}$, also have an uncertainty of ± 0.6 % associated with their calibrations. The values of the measured coupling ratios vary slightly with signal frequency; so a look-up table giving coupling ratios versus frequency is used for the computer calculations of net delivered power. The frequencies listed in the look-up tables are in increments of 50 MHz from 0.2 to 2 GHz and in increments of 100 MHz from 2 to 40 GHz. Linear interpolation is used for signal frequencies which are between two values included in the table. This approach yields interpolated coupling ratio values having an added uncertainty of ± 0.5 %. Therefore, the measurements of $P_{fwd}$ and $P_{rev}$ have a maximum total uncertainty of ± 1.7 %. This represents the sum of 0.6 % for the power meter measurements, 0.6 % for the coupling ratio calibrations, and 0.5 % for possible errors caused by interpolation in the tables of measured coupling ratios. The overall ± 1.7 % uncertainty corresponds to an uncertainty in power delivered to the transmitting antenna ($P_{del}$) of approximately ± 0.07 dB.

The above expressions for $P_{del}$ assume that the directional coupler is ideal. That is, coupling of rf power occurs only between ports 3 and 1, 4 and 2, and 3 and 4 shown in figure 19. Such a coupler is ideal in the sense that there is complete isolation between ports 1 and 4, 2 and 3, and 1 and 2.

## 4.2 Calibration of the Present RF Power Delivery System

A dedicated dual-directional coupler shown in figure 19 is periodically calibrated by one of three different and independent methods at NIST: (1) a six-port power measurement system, which is the present NIST standard for measurement of network parameters, (2) a commercial automatic network analyzer which has been calibrated at NIST, or (3) a procedure in which the coupling ratios are measured with calibrated power meters in our laboratory. Over a period of two years, three sets of coupling ratio measurements were made in 20 MHz increments from 0.2 to 2.0 GHz. These measurements show less than ± 0.06 dB variation (at any given frequency) between the sets of data.

Recently, three sets of coupling ratios were measured from 0.2 to 2.0 GHz, and again the sets differed by less than 0.1 dB.

The periodic NIST calibrations of the power meters and directional couplers constitute the required calibrations for the present rf power delivery system.

## 5. COMPUTATION AND UNCERTAINTY OF THE CHAMBER FIELD MAGNITUDE

Using (1) and the estimated uncertainties for the three quantities appearing on the right side of the equation, the uncertainty in the computed value for the chamber E-field can be calculated. These three uncertainties are discussed separately in the following paragraphs.

The uncertainty in $P_{del}$ can be derived from (7)-(9) written in the form

$$P_{del} = P_{fwd} 10^{[C_{fwd}/10 + A/10]} - P_{rev} 10^{[C_{rev}/10]}, \tag{10}$$

where $P_{fwd}$ and $P_{rev}$ are the readings of the power meters on ports 1 and 2 of the dual-directional coupler in figure 19. When these power meters are calibrated with reference to the NIST primary rf power standard, the measured power has an uncertainty of ± 0.6 %. In the present NIST power delivery method, a high-quality network analyzer is used to measure the two coupling ratios, $C_{fwd}$ and $C_{rev}$, with an uncertainty of ± 0.6 %. As discussed in Section 4.2, an additional possible uncertainty of ± 0.5 % comes from using interpolated values of coupling ratios at frequencies not previously measured. The maximum total possible uncertainty is the sum of these separate uncertainties, or ± 1.7 %, which is approximately ± 0.1 dB.

At the present time, the theoretical (computed) gain values being used in (1) are calculated using (2) for OEGs and (3) for pyramidal horns. For both types of transmitting antennas, the uncertainty of the E-field magnitude in the anechoic chamber, as computed from (1), is ± 0.8 dB. As discussed in Section 3, about half of this uncertainty is caused by multipath interference in the NIST anechoic chamber, and the other half is caused by inaccuracy in determining the effective gain of the transmitting antennas at the near-zone distances used. For purposes of error analysis, we combine the chamber multipath with uncertainty in the free-space antenna gain to obtain the effective uncertainty of ± 0.8 dB for the near-field antenna gain in the anechoic chamber environment.

The total error equation (in dB) relating to (1) is

$$U = 10 \log_{10}(1 + \frac{\Delta P}{P}) + 10 \log_{10}(1 + \frac{\Delta G}{G}) +20 \log_{10}(1 + \frac{\Delta d}{d}), \qquad (11)$$

where $U$ = worst-case uncertainty in the standard E-field generated in the NIST anechoic chamber, ± dB,

$\frac{\Delta P}{P}$ = fractional uncertainty in power delivered to the transmitting antenna,

$\frac{\Delta G}{G}$ = fractional uncertainty in near-zone gain of the transmitting antenna in the anechoic chamber, and

$\frac{\Delta d}{d}$ = fractional uncertainty in measuring the field point distance, for the closest distance used.

The worst-case overall uncertainty in the field strength generated in the anechoic chamber, as calculated from (11) is the sum of ± 0.1 dB for measuring the power P, ± 0.8 dB for calculating the antenna gain G in the anechoic chamber environment, and ± 0.1 dB for measuring the distance d for a total uncertainty of ± 1.0 dB.

The major contributor to possible error is uncertainty in G. Research, both theoretical and experimental, has begun to reduce the uncertainty in both G and d. This involves extensive improvements to the anechoic chamber, including new absorbing material and precise antenna positioners under computer control. This will permit the rapid measurements required for a thorough evaluation of the chamber performance so that accurate corrections can be applied to the theoretically calculated values of field strength for any frequency and field point location used.

## 6. PROCEDURE FOR GENERATING A STANDARD FIELD

The boresight axis of the transmitting antenna in the anechoic chamber is defined by a horizontal laser beam which has been aligned parallel to the direction of motion of the receiving probe cart, as shown in figure 1. The laser is located in the chamber anteroom behind the rolling carriage that supports the transmitting antennas.

To achieve coincidence between the laser alignment beam and the axis of the transmitting antenna, the transmitting antenna is placed on the table located on top of the rolling carriage. The table is then rolled to its maximum forward position into the chamber doorway. The antenna is placed on this table with its aperture 60 cm beyond the plane of the chamber absorber tips. For both OEGs and horns, this aperture plane is far enough inside the chamber so that there are only negligible reflections from the table undercarriage, chamber doorway, and steps into the chamber. The height of the antenna table is then adjusted until the laser beam and boresight axis of the transmitting antenna are at the desired height near the center line. The procedure for an OEG is to align it with the side of the antenna positioner table while the OEG is centered on the laser beam. The OEG is adjusted until its axis is horizontal and in line with the chamber axis. In this way the receiving antenna on the cart can traverse the entire length of the anechoic chamber without becoming misaligned with respect to the laser beam and boresight axis of the transmitting antenna. For the pyramidal horns, the chamber alignment procedure is similar to that described above for OEGs.

Once an OEG or horn has been aligned properly, its boresight axis will be parallel to the direction of motion of the cart. The AUT mounted on the cart in the anechoic chamber is also centered and aligned with respect to the laser beam. The only remaining adjustment to be made is the positioning of the chamber cart at the desired field-point distance.

All instrumentation for the anechoic chamber system is turned on and allowed to stabilize while the transmitting and receiving antennas are being positioned and aligned. Each power meter sensor is calibrated immediately before each set of measurements by connecting it to the internal 1 mW, 50-MHz source built into the power meter.

In the present NIST method of chamber operation, the rf power delivery system is connected to the transmitting antenna by attaching the calibrated directional coupler directly to the antenna. This arrangement puts port 4 of the 4-port system at the coupler-antenna connection as shown in figure 19.

When the transmitter equipment has warmed up and stabilized, the desired field can be established according to the flowchart given in figure 20. The sequence shown there provides the required reading on the forward-power meter in order that the transmitting antenna create the desired field. The output of the rf signal generator is then adjusted until the required reading is attained. In this forward-power determination for a given measurement setup, the only experimental data required is the magnitude of the reflection coefficient at the transmitting antenna input connector. This is determined by setting an arbitrary power level, at the desired frequency, and measuring the forward and reflected power at the side arms of the directional coupler. The power level must be sufficient to avoid noise and zero drift in the power meter indication, but below a power level which could damage the power sensors.

## 7. PLANNED IMPROVEMENTS IN THE ANECHOIC CHAMBER SYSTEM

### 7.1 Transmitting Antenna Positioner

We are now developing a new transmitting antenna positioner. The new positioner and alignment procedure will ensure that the boresight axis of the OEG or the horn is parallel to the direction of cart motion. The new positioner will also improve the repeatability and accuracy of the transmitting antenna position.

## 7.2 Advanced Measurement Software

The basic measurement sequence has been programmed. There are several algorithms that will greatly enhance the overall quality of measurements in the chamber. These include monitoring and leveling the output power and/or measured receiving probe output during the course of a measurement, scanning the boresight direction and determining the optimum location for the calibration, an automated method of applying the system calibration values to reduce the chance for operator errors, and the addition of system monitoring to prevent damage to the sensors and instruments.

## 7.3 Control Charts and Support Software

We are currently developing general control chart software that will help us monitor the measurements and check standard data and the system calibration data. Eventually every component of the system will have a control chart available.

## 7.4 Control Standards

We are planning to produce additional 3 cm and 8 mm open-circuit dipole probes for use as check standards in the chamber. A 15 cm dipole probe is currently in use for frequencies up to 1.0 GHz. A repeatable technique needs to be developed for mounting the check standard in the chamber such that it can be positioned at the calibration location, but can be easily removed and will not interfere with the AUT.

## 7.5 Detailed Uncertainty Analysis

There is a need to reexamine the uncertainty for chamber measurements. The current ± 1 dB might be optimistic for frequencies below 500 MHz, but is probably conservative for frequencies from 18 to 40 GHz [9]. More antenna gain measurements are needed for frequencies below 18 GHz, particularly at the boundaries of the various frequency bands.

## 8. CONCLUSIONS

The NIST anechoic chamber is used to generate standard (known) EM fields for frequencies from 200 MHz to 40 GHz. The present uncertainty of the standard field is the sum of ± 0.1 dB for measuring the power, ± 0.8 dB for calculating the near-field gain of the transmitting antenna, and ± 0.1 dB for measuring the distance from the transmitting antenna for a total uncertainty of ± 1.0 dB. Of the ± 0.8 dB uncertainty in the near-field gain, about half (± 0.4 dB) is due to multipath interference in the NIST anechoic chamber, and the other half (± 0.4 dB) is due to inaccuracy in calculating the gain of the transmitting antenna at the near-field distances used in the chamber.

Some of the planned improvements in the system are a new transmitting antenna positioner, advanced measurement software, control charts and support software, control standards, and a detailed error analysis over the entire frequency range from 200 MHz to 40 GHz. Some measurements between 200 and 500 MHz with OEG transmitting antennas indicate that the uncertainty due to multipath reflections is dependent on the field point location in the chamber, and this needs to be better understood to achieve ± 0.8 dB uncertainty in the near-field antenna gain. On the other hand, measurements from 18 to 40 GHz with pyramidal horns [9] indicate that the chamber reflections are very small and that the uncertainty in the near-field gain is only about ± 0.3 dB in this frequency range.

## 9. REFERENCES


[1] Fitzgerrell, R.G. Using free-space transmission loss for evaluating anechoic chamber performance. IEEE Trans. Electromag. Compat., EMC-24: 356-358; 1982.

[2] Kanda, M.; Wyss, J.C. Evaluation of off-axis measurements performed in an anechoic chamber. Nat. Bur. Stand. (U.S.) Tech. Note 1305; 1986.

[3] Larsen, E.B.; Ries, F.X. Design and calibration of the NBS isotropic electric-field monitor (EFM-5), 0.2 to 1000 MHz. Nat. Bur. Stand. (U.S.) Tech. Note 1033; 1981.

[4] Bowman, R.R. Calibration techniques for electromagnetic hazard meters: 500 MHz to 20 GHz. Nat. Bur. Stand. (U.S.) NBSIR 75-805; 1975.

[5] Wu, D.I.; Kanda, M. Comparison of theoretical and experimental data for the near field of an open-ended rectangular waveguide. IEEE Trans. Electromag. Compat., 31: 353-358; 1989.

[6] Jull, E.V. Finite-range gain of sectoral and pyramidal horns. Electronics Letters, 6: 680-681; 1970.

[7] Jull, E.V. Aperture Antennas and Diffraction Theory. Stevenage: Peter Peregrinus Ltd.; 1981.

[8] Boersma, J. Computation of Fresnel integrals. Math. Comp., 14: 380; 1960.

[9] Hill, D.A.; Ehret, R.L. Near-field gain of pyramidal horns from 18 to 40 GHz. Nat. Inst. Stand. Tech. (U.S.) NISTIR 89-3924; 1989.

[10] Kanda, M.; Orr, R.D. A radio-frequency power delivery system: procedures for error analysis and self-calibration. Nat. Bur. Stand. (U.S.) Tech. Note 1083; 1985.

Table 1. Anechoic chamber reflection errors for 1 to 3 m separation distances. *

| Frequency MHz | Source Antenna | Probe Dipole Length cm or OEG Size | Range of Error dB | Uncertainty dB |
|---|---|---|---|---|
| 175 OEG | WR 3600 | 30 | -0.6,+0.1 | ±0.10 |
| 229 | WR 3600 | 30 | -0.6,+0.5 | ±0.14 |
| 301 | WR 3600 | 30 | -0.5,+0.2 | ±0.10 |
| 394 | WR 2100 | 15 | -0.4,+0.2 | ±0.08 |
| 517 | WR 2100 | 15 | -0.3,+0.2 | ±0.08 |
| 517 HORN | SA 12-0.5 | 15 | -0.3,+0.1 | ±0.06 |
| 677 | SA 12-0.5 | 15 | -0.3,+0.1 | ±0.06 |
| 888 | SA 12-0.75 | 15 | -0.2,+0.1 | ±0.06 |
| 1164 | NARDA 646 | 10 | -0.2,+0.2 | ±0.06 |
| 1527 | NARDA 646 | 10 | -0.2,+0.0 | ±0.04 |
| 2000 | NARDA 645 | 10 | ±0.1 | ±0.04 |
| 2450 | NARDA 645 | 3.3 | ±0.1 | ±0.04 |
| 3950 | MICROLAB S638A | 3.3 | ±0.1 | ±0.04 |
| 4000 | MICROLAB H638A | WR 187 | ±0.04 | ±0.03 |
| 5000 | MICROLAB H638A | WR 187 | ±0.12 | ±0.04 |
| 6100 | SA 12-5.8 | WR 137 | ±0.04 | ±0.03 |
| 7600 | SA 12-5.8 | WR 137 | ±0.04 | ±0.03 |
| 9400 | DBG-520-20 | WR 90 | ±0.05 | ±0.03 |
| 11700 | DBG-520-20 | WR 90 | ±0.04 | ±0.03 |
| 14500 | SA 12-12 | WR 62 | ±0.04 | ±0.03 |
| 18000 | SA 12-12 | WR 62 | ±0.04 | ±0.03 |

* Certain commercial equipment, instruments, or materials are identified in this paper in order to adequately specify the experimental procedure. Such identification does not imply recommendation or endorsement by the National Institute of Standards and Technology, nor does it imply that the materials or equipment identified are necessarily the best available for the purpose.

Table 2. Error due to off-axis alignment.

| Offset distance from center line (m) | | 0.25 (dB) | 0.50 (dB) | 0.75 (dB) | 1.00 (dB) |
|---|---|---|---|---|---|
| Frequency (MHz) | Source Antenna type | | | | |
| 250 | OEG | | | | ±0.8 |
| 600 | Horn | | | | ±2.5 |
| 700 | Horn | | | | ±2.5 |
| 800 | Horn | | | | ±2.5 |
| 900 | Horn | ±0.5 | ±1.2 | ±2.0 | ±2.5 |
| 1000 | Horn | | | | ±3.0 |

Table 3. Dimensions and frequencies of OEG antennas.

1. WR-3600 Open-Ended Guide
   Frequency = 200 to 300 MHz
   Aperture = 91.44 cm x 45.72 cm (36 in x 18 in)

2. WR-2100 Open-Ended Guide
   Frequency = 300 to 500 MHz
   Aperture = 53.34 cm x 26.67 cm (21 in x 10.5 in)

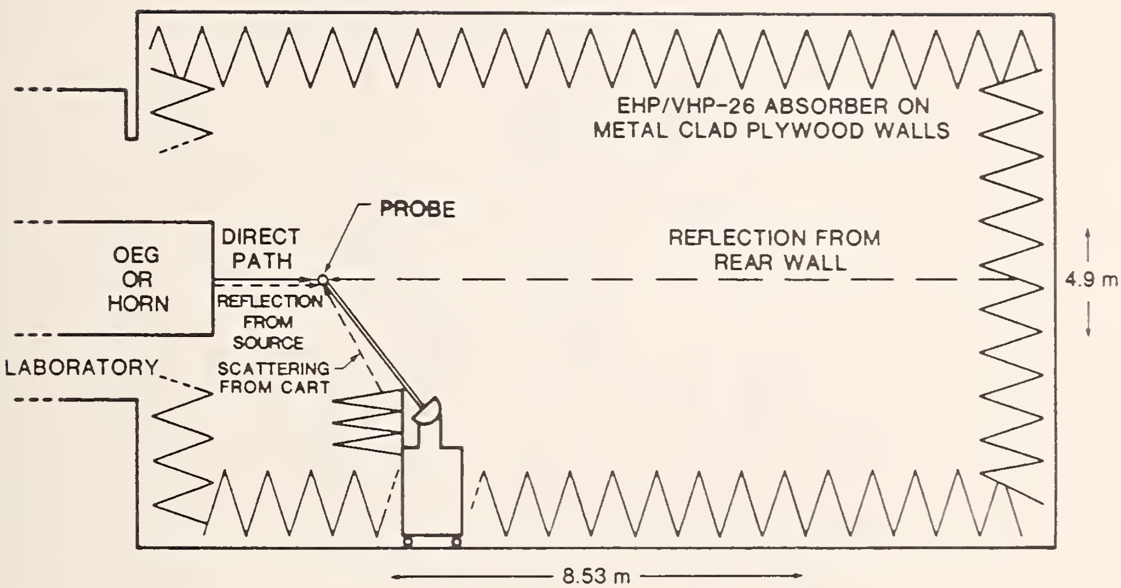


Figure 1. A side view of the NIST-Boulder anechoic chamber.

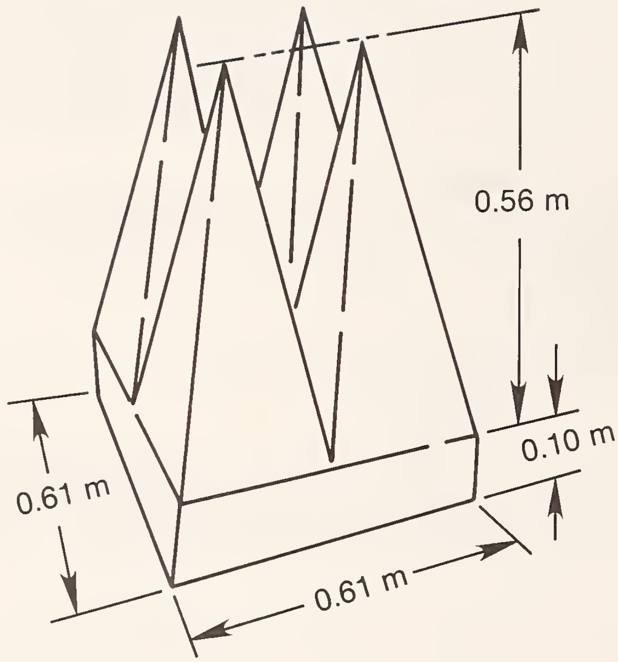


Figure 2. Carbon-impregnated urethane foam which lines the walls, ceiling, and floor of the anechoic chamber.

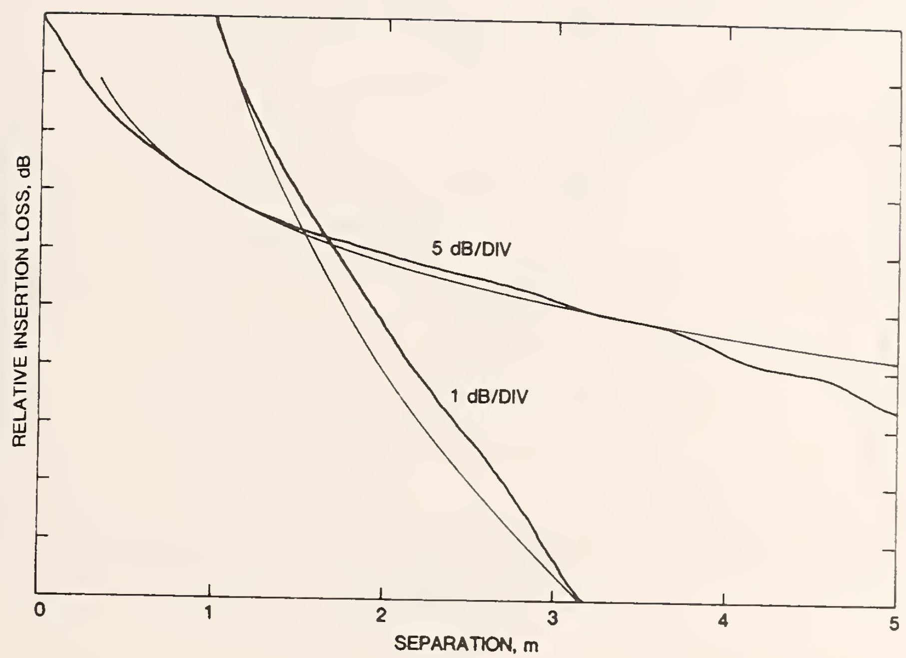


Figure 3. Relative insertion loss between source and probe antenna versus separation distance with free-space transmission loss curve fitted at 1 m; frequency = 175 MHz; OEG source antenna.

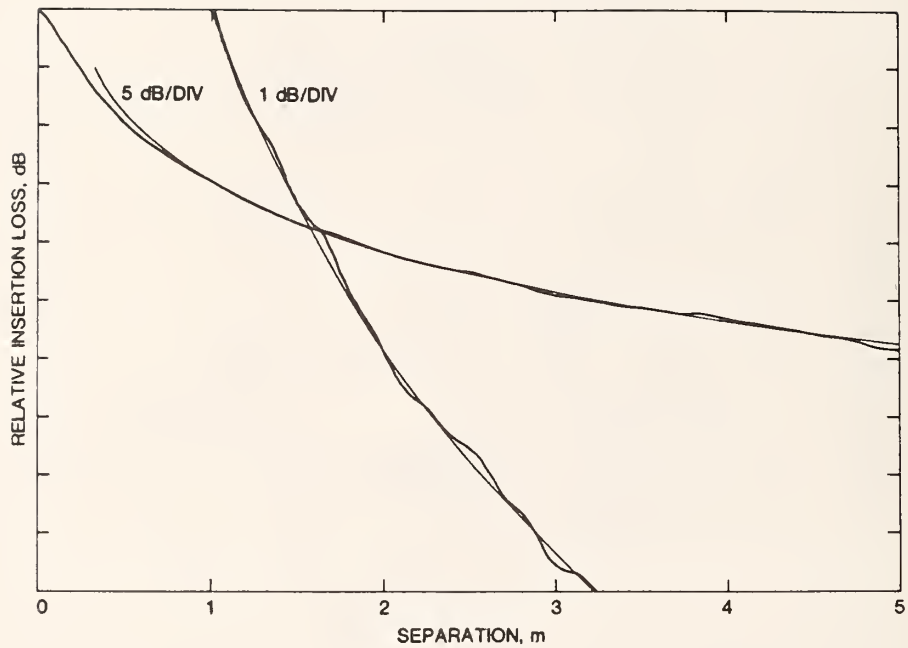


Figure 4. Relative insertion loss between source and probe antenna versus separation distance with free-space transmission loss curve fitted at 1 m; frequency = 517 MHz; OEG source antenna.

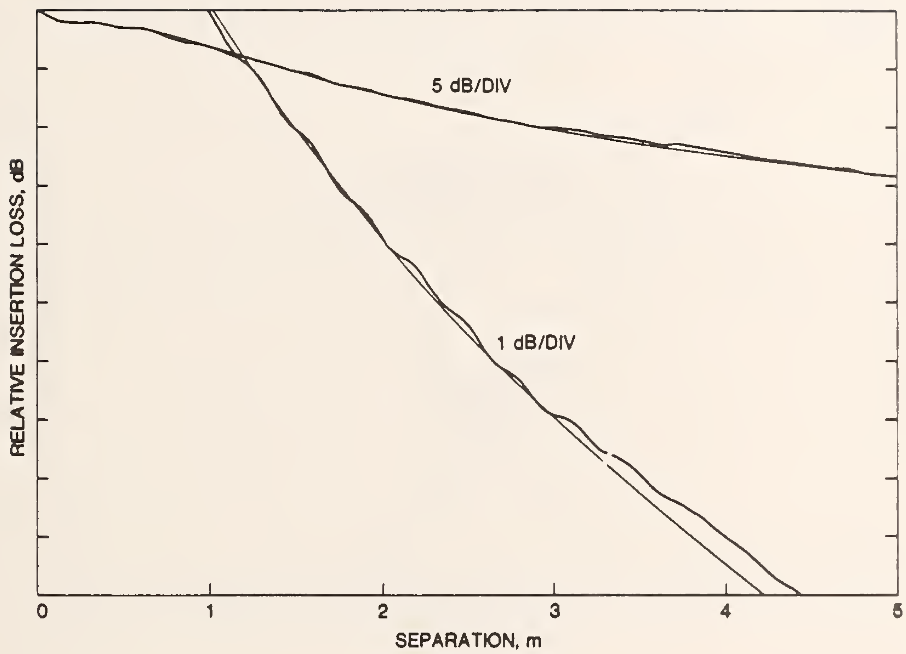


Figure 5. Relative insertion loss between source and probe antenna versus separation distance with free-space transmission loss curve fitted at 1 m; frequency = 517 MHz; horn source antenna.

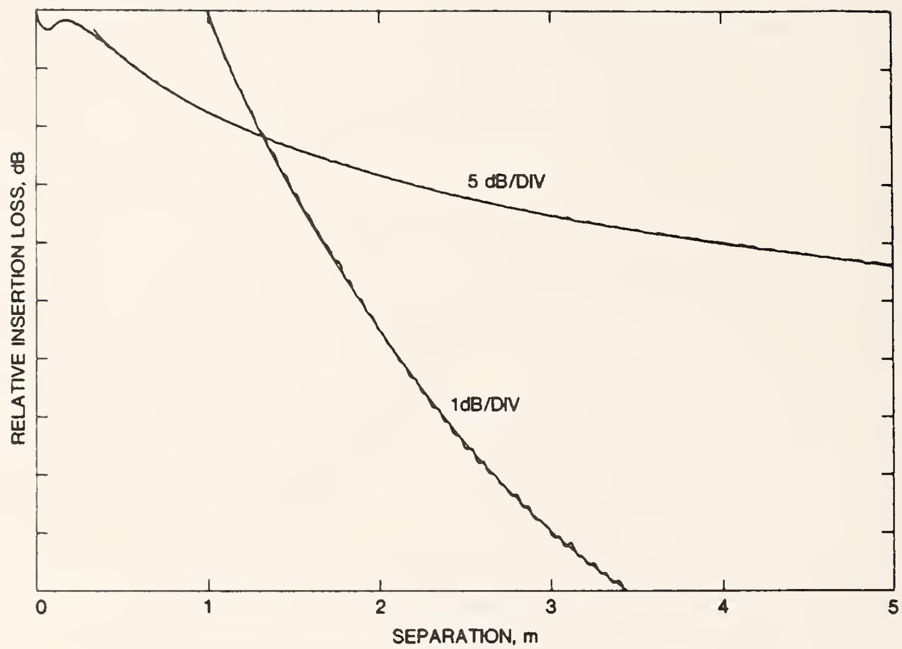


Figure 6. Relative insertion loss between source and probe antenna versus separation distance with free-space transmission loss curve fitted at 1 m; frequency = 2450 MHz; horn source antenna.

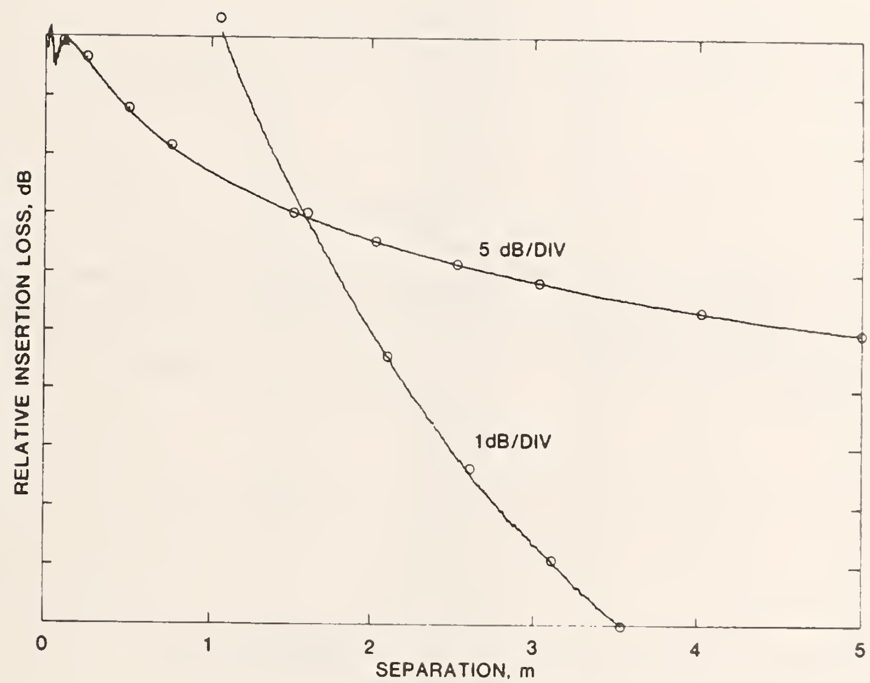


Figure 7. Relative insertion loss between source and probe antenna versus separation distance with free-space transmission loss curve fitted at 1 m; frequency = 11 700 MHz; horn source antenna. Note: Difference between measured and calculated data point on 1-dB/div curve at 1-m separation is caused by cart inertia.

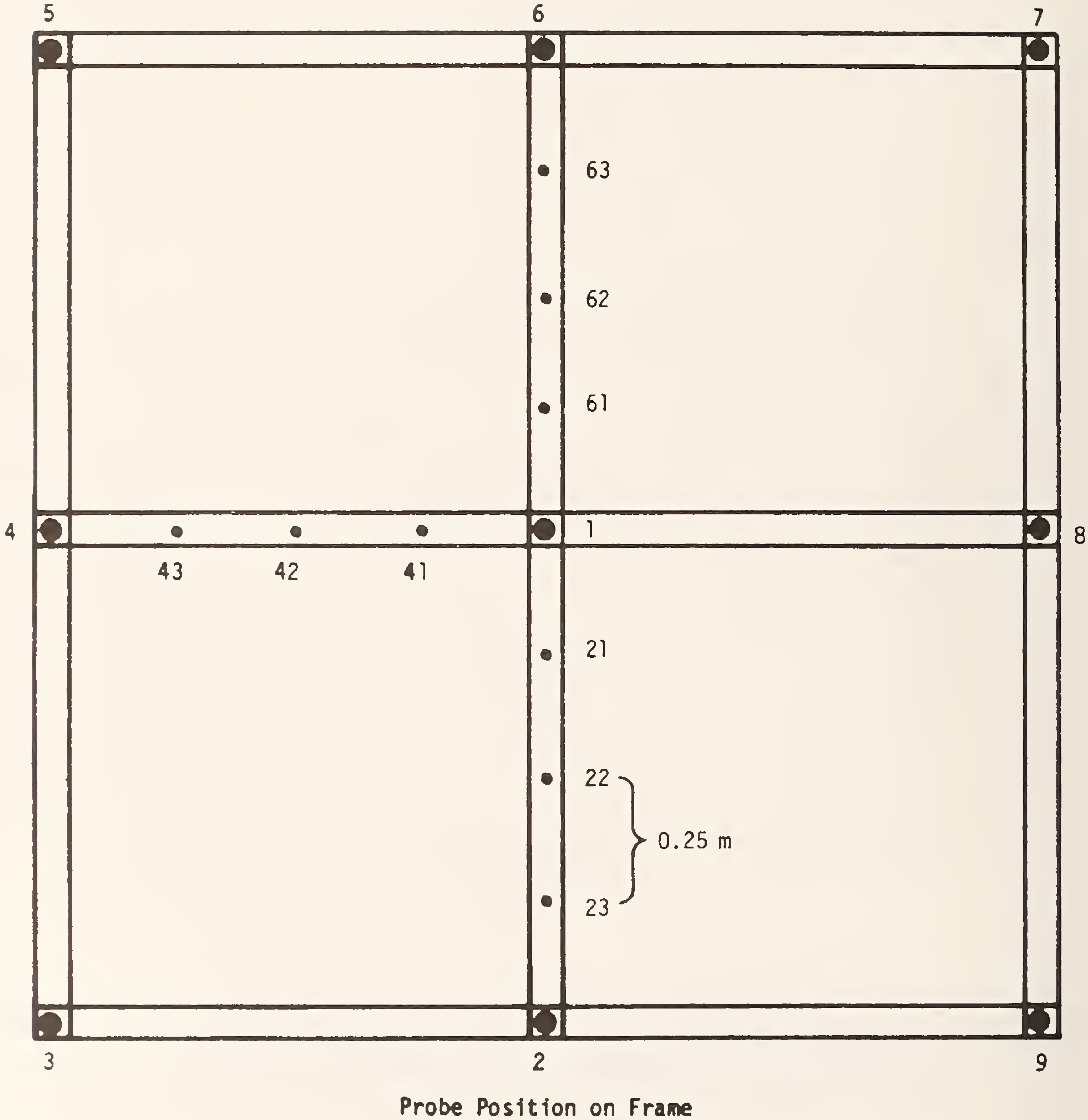


Figure 8. Frame used for holding probe on cart. Positions 1 through 9 are separated by 1 m intervals. The numbered positions (21-24, 41-44, and 61-64) are each separated by 25 cm.

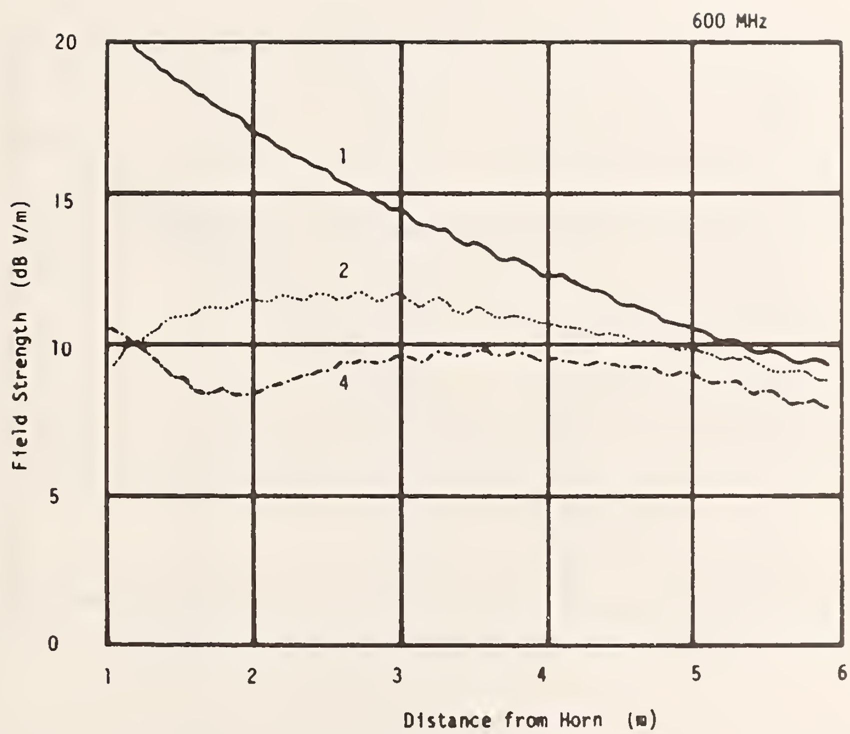


Figure 9. Field strength versus distance from horn for 1 m off-axis position at 600 MHz.

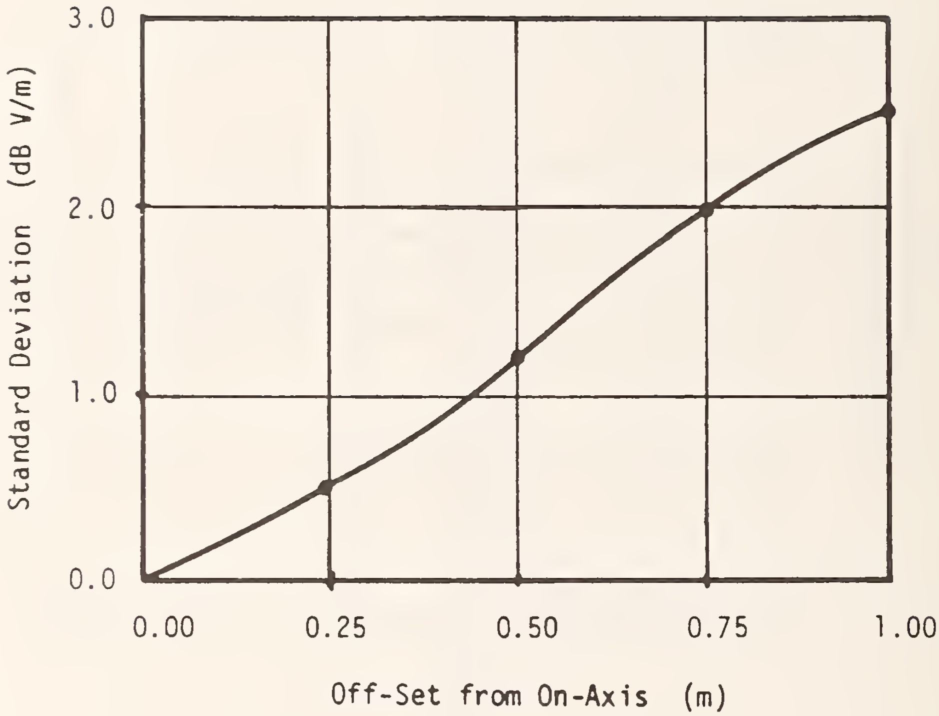


Figure 10. Standard deviation of the electric field versus offset from center line at 800 MHz. In each case, the worst case standard deviation is used for distances more than 2 m from the launching horn.

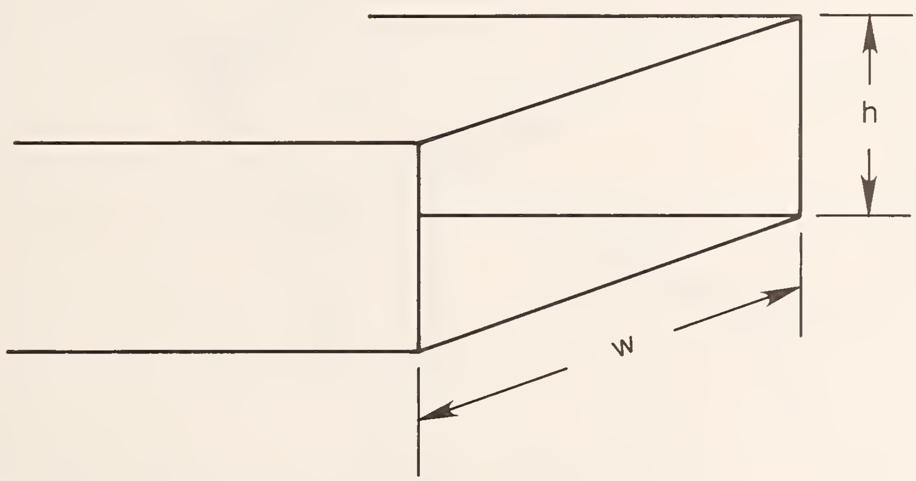


Figure 11. Geometry for an open-ended rectangular waveguide.

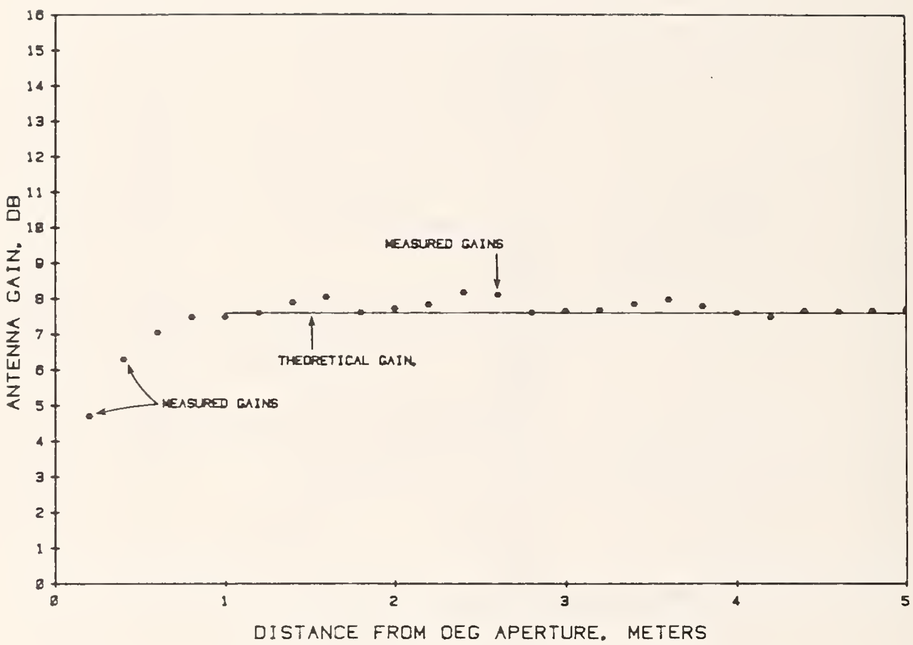


Figure 12. WR-2100 OEG gain vs distance at 500 MHz.

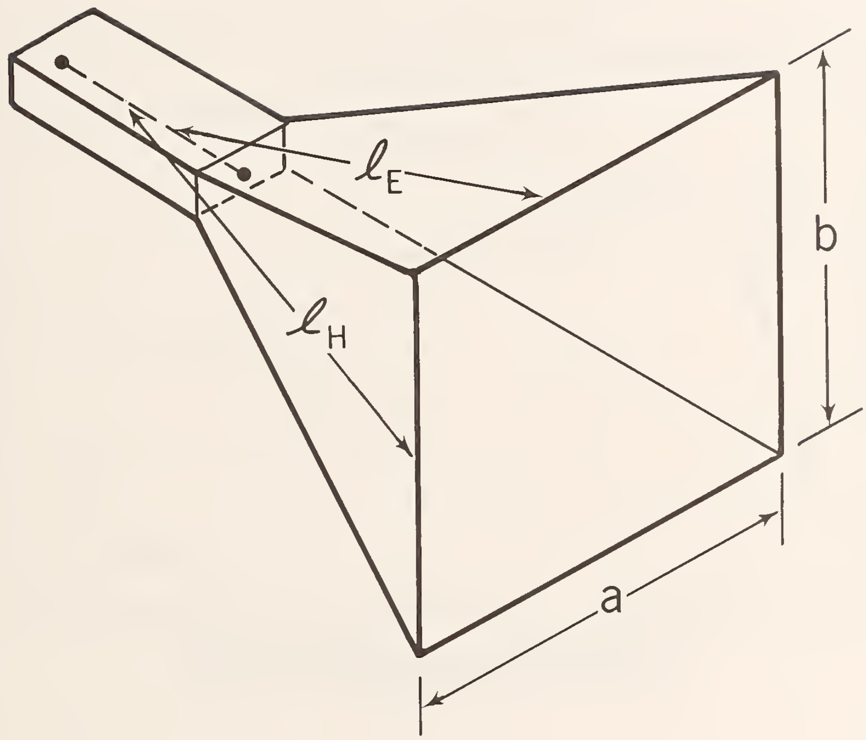


Figure 13. Geometry for a pyramidal horn.

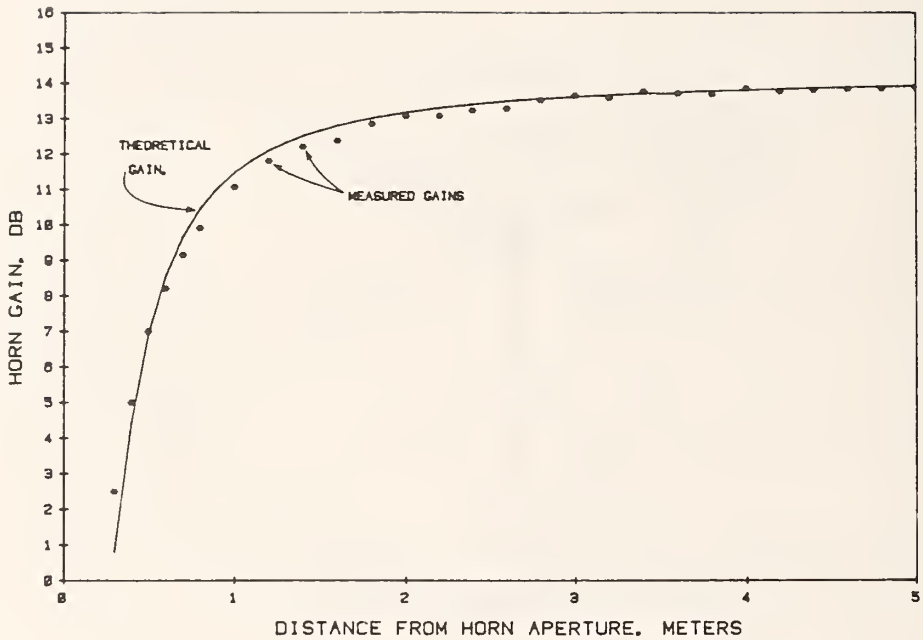


Figure 14. Pyramidal horn gain vs distance at 500 MHz. Horn dimensions: a = 122.5 cm, b = 90.75 cm, $\ell_H$ = 142.0 cm, $\ell_E$ = 121.3 cm.

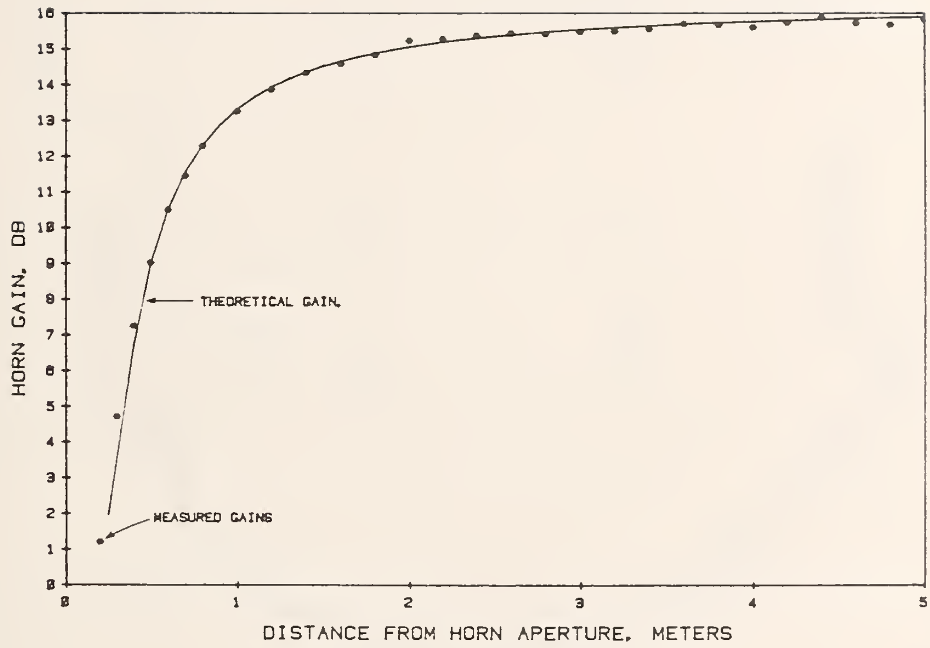


Figure 15. Pyramidal horn gain vs distance at 1000 MHz. Horn dimensions: a = 82.78 cm, b = 61.18 cm, $\ell_H$ = 94.3 cm, $\ell_E$ = 81.2 cm.

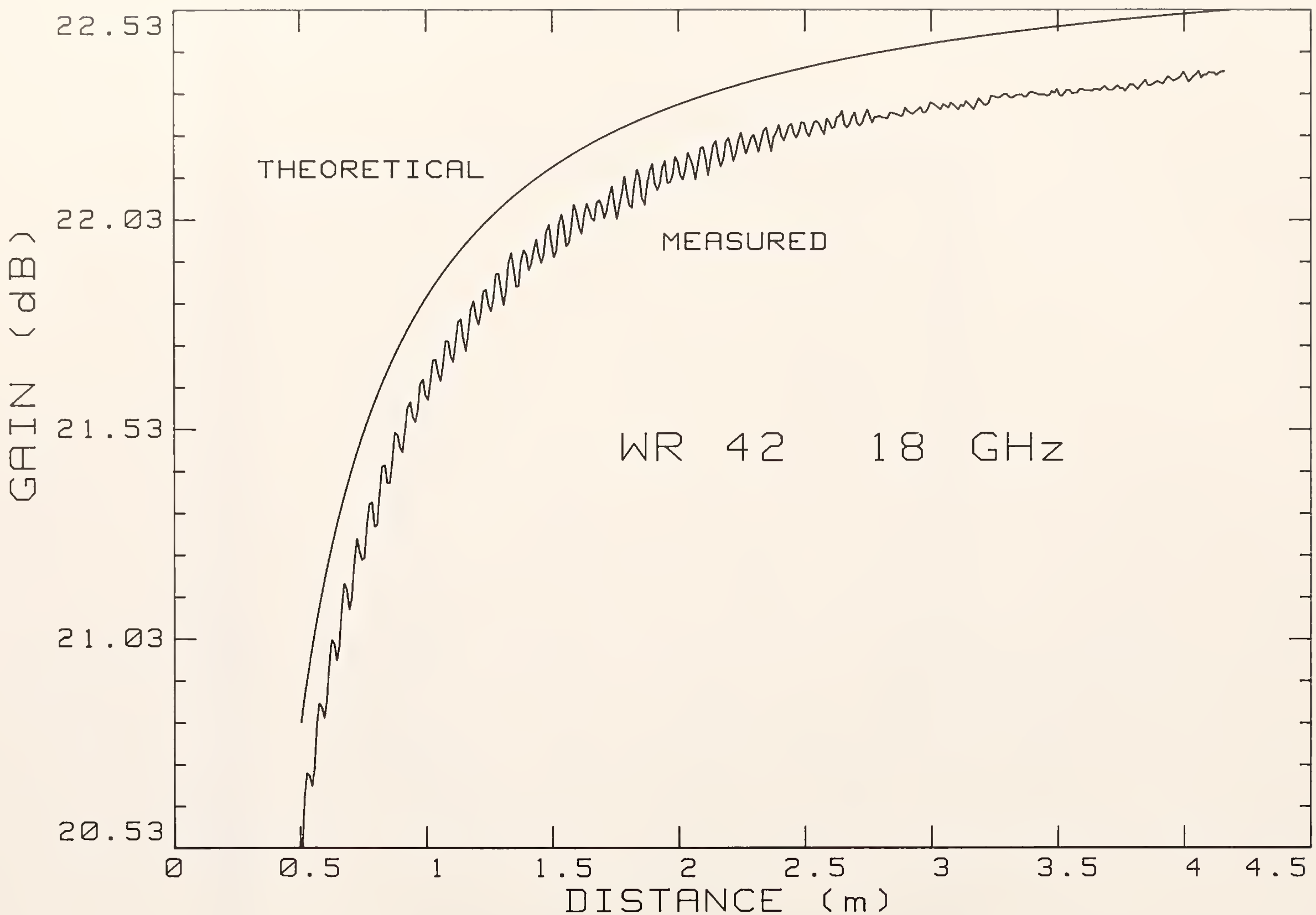


Figure 16. Pyramidal horn gain vs distance at 18 GHz. Horn dimensions: a = 10.43 cm, b = 7.88 cm, $\ell_H$ = 20.34 cm, $\ell_E$ = 19.09 cm.

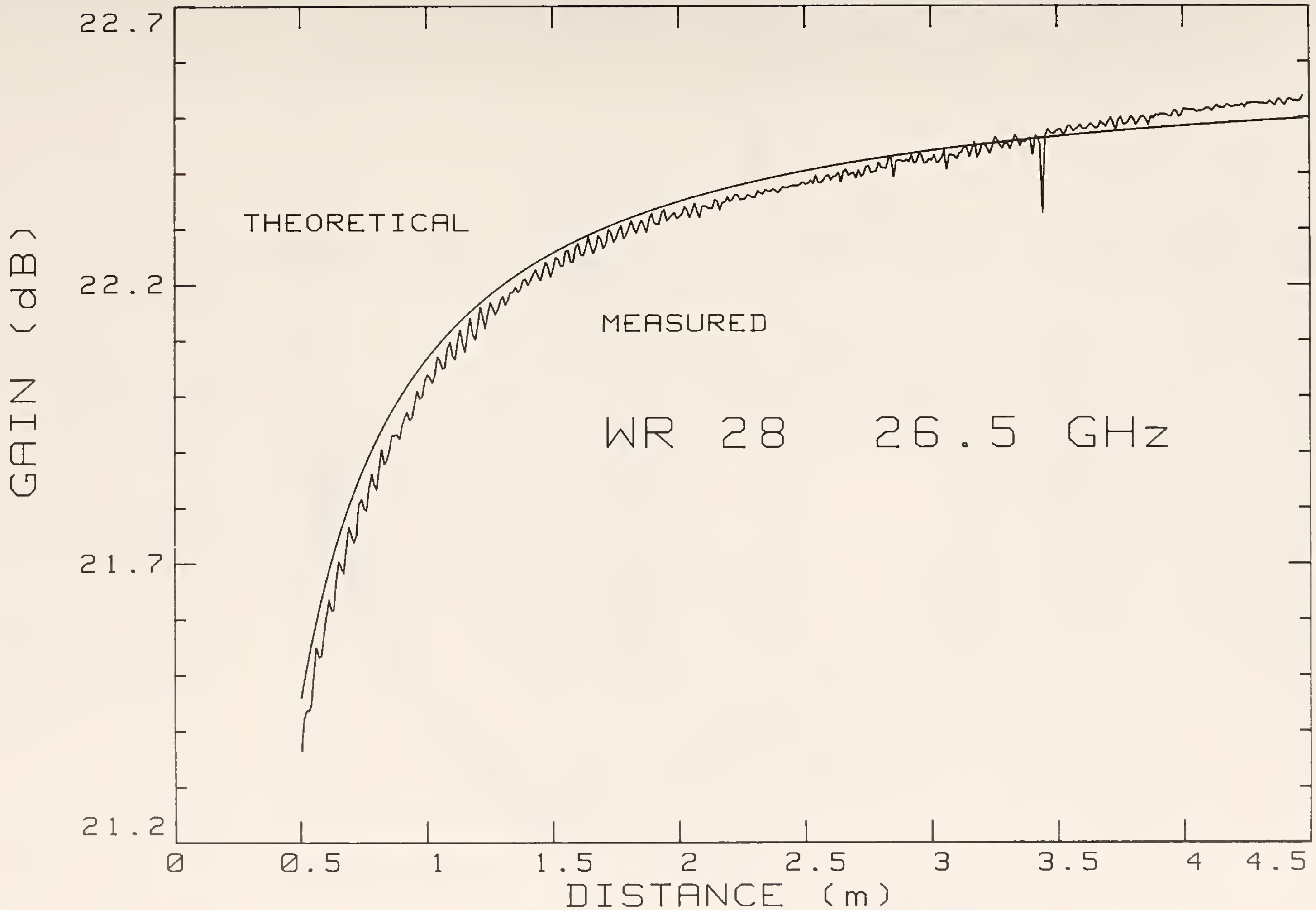


Figure 17. Pyramidal horn gain vs distance at 26.5 GHz. Horn dimensions: $a = 6.89$ cm, $b = 5.27$ cm, $\ell_H = 14.00$ cm, $\ell_E = 12.73$ cm.

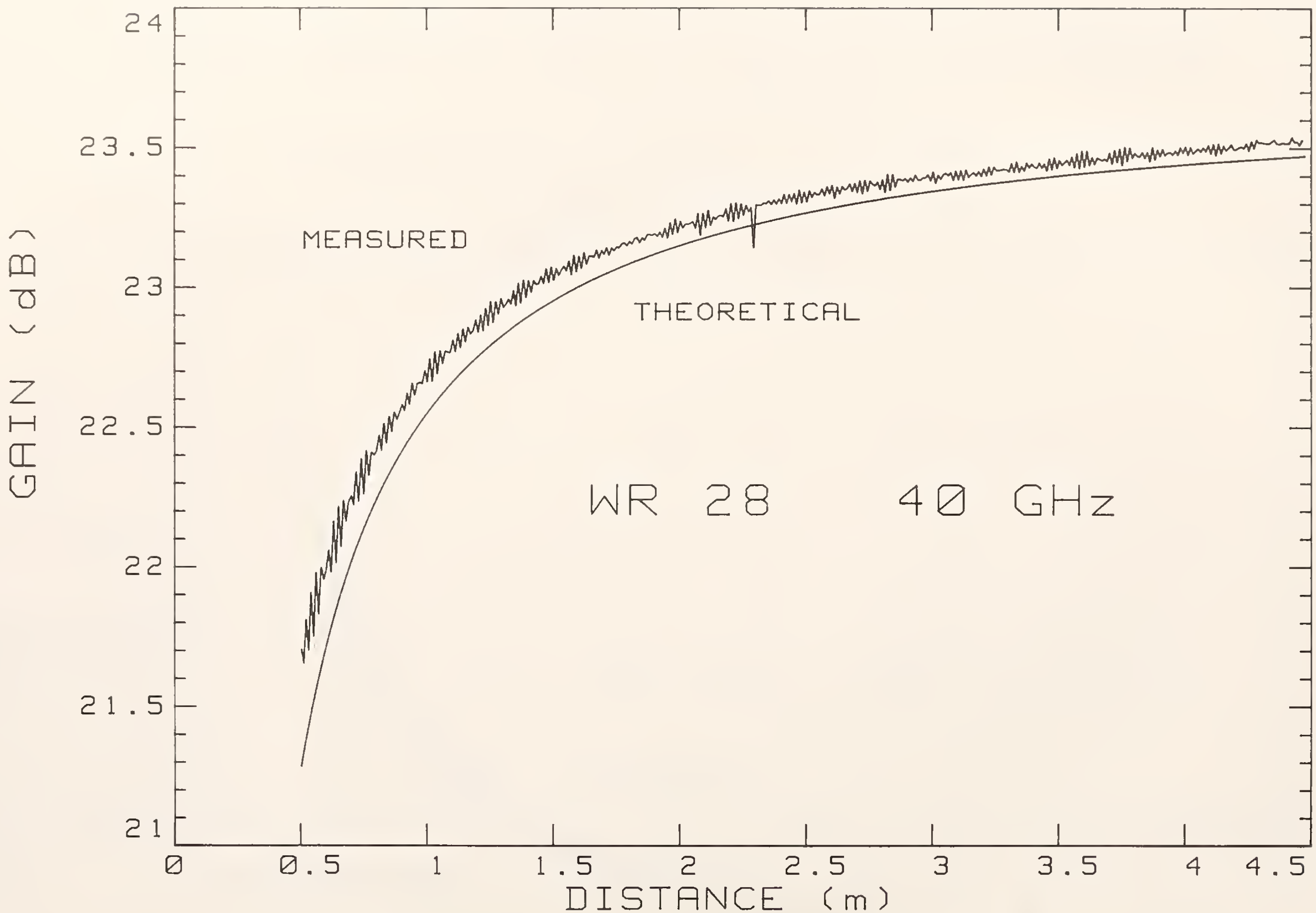


Figure 18. Pyramidal horn gain vs distance at 40 GHz. Horn dimensions: a = 6.89 cm, b = 5.27 cm, $\ell_H$ = 14.00 cm, $\ell_E$ = 12.73 cm.

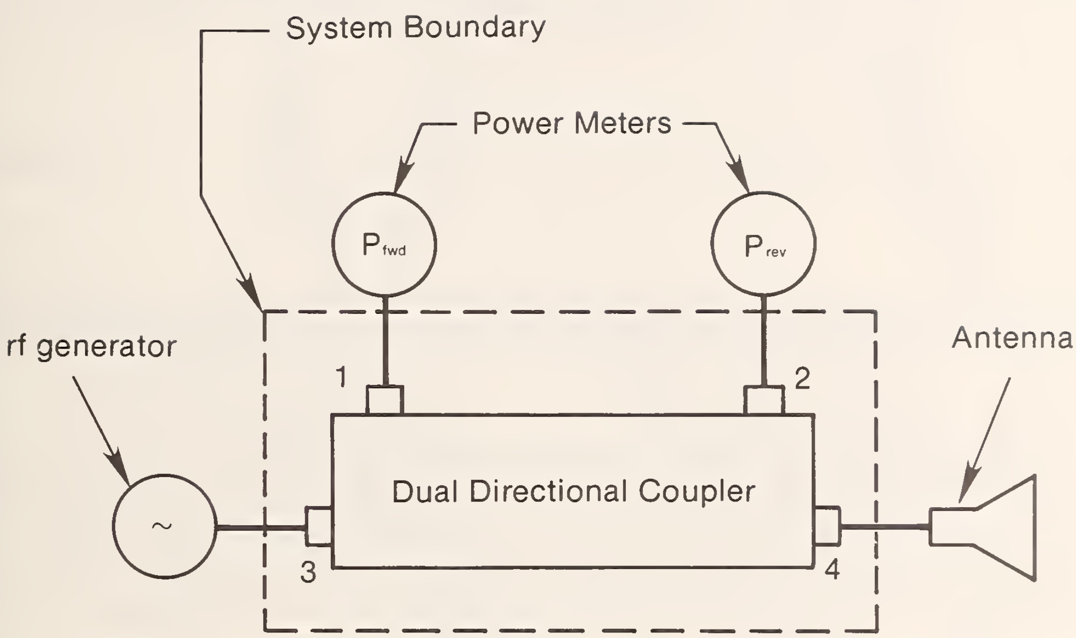


Figure 19. System for measuring rf power delivered to an antenna.

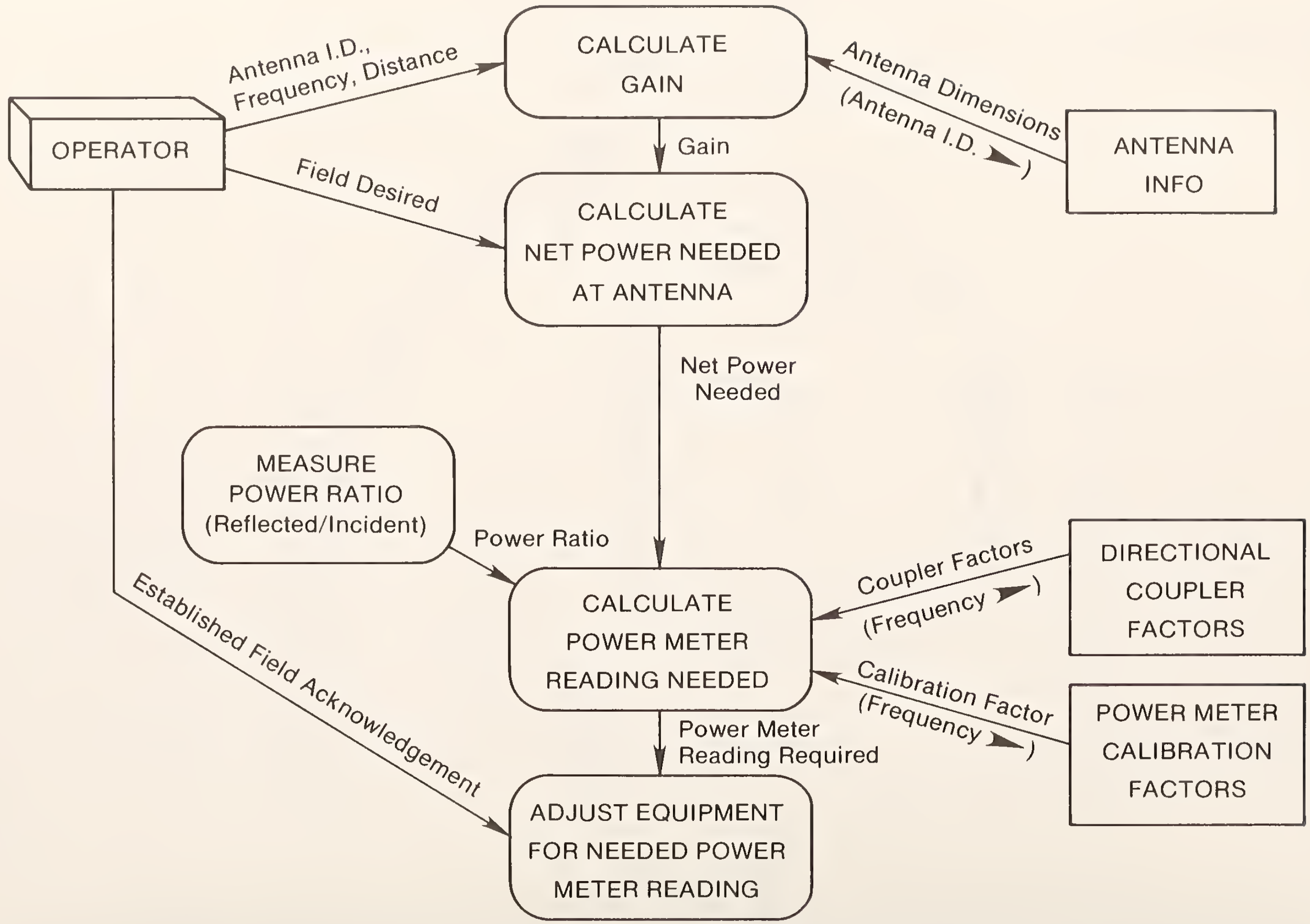


Figure 20. Flow diagram for producing a known boresight field strength in the anechoic chamber.

NIST-114A (REV. 3-89)

U.S. DEPARTMENT OF COMMERCE
NATIONAL INSTITUTE OF STANDARDS AND TECHNOLOGY

# BIBLIOGRAPHIC DATA SHEET

1. PUBLICATION OR REPORT NUMBER: NIST/TN-1335
2. PERFORMING ORGANIZATION REPORT NUMBER:
3. PUBLICATION DATE: March 1990

4. TITLE AND SUBTITLE

Generating Standard Reference Electromagnetic Fields in the NIST Anechoic Chamber, 0.2 to 40 GHz

5. AUTHOR(S)

D.A. Hill, M. Kanda, E.B. Larsen, G.H. Koepke, and R.D. Orr

6. PERFORMING ORGANIZATION (IF JOINT OR OTHER THAN NIST, SEE INSTRUCTIONS)

U.S. DEPARTMENT OF COMMERCE
NATIONAL INSTITUTE OF STANDARDS AND TECHNOLOGY
~~GAITHERSBURG, MD 20899~~ Boulder, Colorado 80303-3328

7. CONTRACT/GRANT NUMBER

8. TYPE OF REPORT AND PERIOD COVERED

9. SPONSORING ORGANIZATION NAME AND COMPLETE ADDRESS (STREET, CITY, STATE, ZIP)

10. SUPPLEMENTARY NOTES

☐ DOCUMENT DESCRIBES A COMPUTER PROGRAM; SF-185, FIPS SOFTWARE SUMMARY, IS ATTACHED.

11. ABSTRACT (A 200-WORD OR LESS FACTUAL SUMMARY OF MOST SIGNIFICANT INFORMATION. IF DOCUMENT INCLUDES A SIGNIFICANT BIBLIOGRAPHY OR LITERATURE SURVEY, MENTION IT HERE.)

The NIST anechoic chamber is used to generate standard (known) EM fields for frequencies from 200 MHz to 40 GHz. The transmitting antennas used are open-ended rectangular waveguides from 200 to 500 MHz and pyramidal horns from 450 MHz to 40 GHz. The uncertainty in the electric field is currently estimated to be $\pm 1.0$ dB. A number of changes and additions are planned to improve the accuracy, repeatability, and efficiency of the system.

12. KEY WORDS (6 TO 12 ENTRIES; ALPHABETICAL ORDER; CAPITALIZE ONLY PROPER NAMES; AND SEPARATE KEY WORDS BY SEMICOLONS)

anechoic chamber; delivered power; near-field gain; open-ended waveguide; pyramidal horn; standard field

13. AVAILABILITY

- [X] UNLIMITED
- [ ] FOR OFFICIAL DISTRIBUTION. DO NOT RELEASE TO NATIONAL TECHNICAL INFORMATION SERVICE (NTIS).
- [X] ORDER FROM SUPERINTENDENT OF DOCUMENTS, U.S. GOVERNMENT PRINTING OFFICE, WASHINGTON, DC 20402.
- [ ] ORDER FROM NATIONAL TECHNICAL INFORMATION SERVICE (NTIS), SPRINGFIELD, VA 22161.

14. NUMBER OF PRINTED PAGES: 48

15. PRICE

ELECTRONIC FORM

# NIST Technical Publications

## *Periodical*

**Journal of Research of the National Institute of Standards and Technology**—Reports NIST research and development in those disciplines of the physical and engineering sciences in which the Institute is active. These include physics, chemistry, engineering, mathematics, and computer sciences. Papers cover a broad range of subjects, with major emphasis on measurement methodology and the basic technology underlying standardization. Also included from time to time are survey articles on topics closely related to the Institute's technical and scientific programs. Issued six times a year.

## *Nonperiodicals*

**Monographs**—Major contributions to the technical literature on various subjects related to the Institute's scientific and technical activities.

**Handbooks**—Recommended codes of engineering and industrial practice (including safety codes) developed in cooperation with interested industries, professional organizations, and regulatory bodies.

**Special Publications**—Include proceedings of conferences sponsored by NIST, NIST annual reports, and other special publications appropriate to this grouping such as wall charts, pocket cards, and bibliographies.

**Applied Mathematics Series**—Mathematical tables, manuals, and studies of special interest to physicists, engineers, chemists, biologists, mathematicians, computer programmers, and others engaged in scientific and technical work.

**National Standard Reference Data Series**—Provides quantitative data on the physical and chemical properties of materials, compiled from the world's literature and critically evaluated. Developed under a worldwide program coordinated by NIST under the authority of the National Standard Data Act (Public Law 90-396). NOTE: The Journal of Physical and Chemical Reference Data (JPCRD) is published quarterly for NIST by the American Chemical Society (ACS) and the American Institute of Physics (AIP). Subscriptions, reprints, and supplements are available from ACS, 1155 Sixteenth St., NW., Washington, DC 20056.

**Building Science Series**—Disseminates technical information developed at the Institute on building materials, components, systems, and whole structures. The series presents research results, test methods, and performance criteria related to the structural and environmental functions and the durability and safety characteristics of building elements and systems.

**Technical Notes**—Studies or reports which are complete in themselves but restrictive in their treatment of a subject. Analogous to monographs but not so comprehensive in scope or definitive in treatment of the subject area. Often serve as a vehicle for final reports of work performed at NIST under the sponsorship of other government agencies.

**Voluntary Product Standards**—Developed under procedures published by the Department of Commerce in Part 10, Title 15, of the Code of Federal Regulations. The standards establish nationally recognized requirements for products, and provide all concerned interests with a basis for common understanding of the characteristics of the products. NIST administers this program as a supplement to the activities of the private sector standardizing organizations.

**Consumer Information Series**—Practical information, based on NIST research and experience, covering areas of interest to the consumer. Easily understandable language and illustrations provide useful background knowledge for shopping in today's technological marketplace.

*Order the* **above** *NIST publications from: Superintendent of Documents, Government Printing Office, Washington, DC 20402.*

*Order the* **following** *NIST publications—FIPS and NISTIRs—from the National Technical Information Service, Springfield, VA 22161.*

**Federal Information Processing Standards Publications (FIPS PUB)**—Publications in this series collectively constitute the Federal Information Processing Standards Register. The Register serves as the official source of information in the Federal Government regarding standards issued by NIST pursuant to the Federal Property and Administrative Services Act of 1949 as amended, Public Law 89-306 (79 Stat. 1127), and as implemented by Executive Order 11717 (38 FR 12315, dated May 11, 1973) and Part 6 of Title 15 CFR (Code of Federal Regulations).

**NIST Interagency Reports (NISTIR)**—A special series of interim or final reports on work performed by NIST for outside sponsors (both government and non-government). In general, initial distribution is handled by the sponsor; public distribution is by the National Technical Information Service, Springfield, VA 22161, in paper copy or microfiche form.

**U.S. DEPARTMENT OF COMMERCE**
National Institute of Standards and Technology
(formerly National Bureau of Standards)
325 Broadway
Boulder, Colorado 80303-3328